

A High-Speed Time-Optimal Trajectory Generation Strategy via a Two-Layer Planning Model[★]

Haotian Tan, Yuan-Hua Ni

College of Artificial Intelligence, Nankai University, Tianjin 300350, PR China

Abstract

Motion planning and trajectory generation are crucial technologies in various domains including the control of Unmanned Aerial Vehicles, manipulators, and rockets. However, optimization-based real-time motion planning becomes increasingly challenging due to the problem's probable non-convexity and the inherent limitations of non-linear programming algorithms. Highly nonlinear dynamics, obstacle avoidance constraints, and non-convex inputs can exacerbate these difficulties. In order to enhance the robustness and reduce the computational burden, this paper proposes a two-layer trajectory generating algorithm for intelligent ground vehicles with convex optimization methods, aiming to provide real-time guarantees for trajectory optimization and to improve the calculate speed of motion prediction. Our approach involves breaking down the original problem into small horizon-based planning cycles with fixed final times, referred to as planning cycles. Each planning cycle is then solved within a series of restricted convex sets constructed by some customized search algorithms incrementally. We rigorously establish these advantages through mathematical analysis under moderate assumptions and comprehensive experimental validations. For linear vehicle models, comparative experiments with general sequential convex programming algorithms demonstrate the superior performance of our proposed method, particularly in terms of the computational efficiency in dynamic maps and the reduced final time.

Key words: Trajectory optimization; convex programming; artificial potential field

1 Introduction

As industrial technology continues to evolve, numerous automobile devices have emerged, giving rise to trajectory generation as a vital realm of research. Trajectory generation and motion planning aim to find proper control for agents such as robots, drones, or other autonomous systems to navigate from one location to another while avoiding obstacles. An efficient trajectory planning method is essential since it can significantly save energy or time while guarantee the safeness, ultimately resulting in substantial financial savings.

Over the past few decades, a variety of planning algorithms have emerged. Despite their differing methodologies and distinct application scenarios, these methods can be broadly categorized into three primary categories [1]: The search-based methods, the sampling-based and the optimization-based ones. For the search-based algorithms, the well-known A* is first introduced in 1968 [2]. It efficiently finds optimal paths by ap-

plying heuristic functions [3][4][5][6], but suffers from high computational costs in large-scale problems with dense grids [7]. Subsequent improvements include D* [8], which enables dynamic path replanning when encountering new obstacles, and ARA* [9], which optimizes efficiency through search reuse. While these variants enhance adaptability, they inherit A*'s fundamental scalability limitations, restricting their application in large-scale real-time systems. On the field of the sampling-based algorithms, the rapidly-exploring random Tree (RRT) algorithm provides an efficient framework for obstacle avoidance through probabilistic space exploration [10][11]. While basic RRT offers simplicity and flexibility, its extension RRT* [12] achieves asymptotic optimality at increased computational cost. Although numerous RRT variants have demonstrated scenario-specific advantages in diverse applications [13][14], the limitation of hardware and kinematic-infeasibility still confine the wide use of these variations. During the past few decades, there are also vast studies that tackle planning problems with optimization techniques. Indirect methods, such as those based on Pontryagin's maximum principle or Lagrange multipliers [15][16], provide analytical solutions but face computational challenges due to sensitivity to initial conditions and implementation dif-

[★] This work is supported in part by the National Natural Science Foundation of China (62173191)

Email addresses: ElmundoTan@outlook.com (Haotian Tan), yhni@nankai.edu.cn (Yuan-Hua Ni).

ficulties. In contrast, direct methods remodel the optimal control problem with nonlinear programming (NLP) problems through discretization, permitting numerical solution via gradient-based (e.g., Newton's method [17]) or heuristic (e.g., genetic algorithms) approaches. Although general NLP problems are NP-hard, significant progress has been made through convexification techniques that enable efficient solutions for specific problem classes, since convex problems are easy to solve. For some non-convex inputs such as the positive minimal thrust constraints in the rocket model, apply the lossless convex relaxation technique to broaden the original control vector could transform the non-convex input constraints into convex ones [18][19][20]. Despite the extra variables being introduced, it can be guaranteed that the relaxed problems become easier to solve benefits from its convex structure. For problems with non-convex state constraints such as obstacle avoidance constraints, sequential optimization algorithms can be applied to find a feasible trajectory quickly [21], while it may result in obtaining an undesirable solution during iterations [22]. Correspondingly, adding trast region constraints, using stricter approximated constraints and transferring the hard constraints to soft ones can reduce the risk of ill-conditioned solutions and alleviate the so-called artificial infeasibility respectively [23].

These direct optimization methods are widely employed in time-optimal control problems. The modelling process for fixed-time step problems is relatively straightforward, which enables us to transform free final time problems into a series of fixed-final time optimization subproblems, and a line search program can be applied to obtain a proper trajectory from the solution of those subproblems [24]. Time-optimal control problems can also be settled by solving fixed-time optimal subproblems successively [25]. However, this approach relies heavily on the availability of extensive map information and lacks final constraints, which may limit its applicability.

This paper focuses on a collision-free trajectory generating problems with static or moving obstacles. In order to improve the quality and time optimality of the solutions in motion planning, we propose a dynamic trajectory generation algorithm that is rooted in an iterative two-layer optimization procedure. In each iteration, a planning cycle featuring a short fixed final time is employed, with each cycle further divided into two trajectory optimization problems and an associated trajectory searching algorithm. By incrementally generating segmented control inputs, an entire control can be obtained with dynamic obstacle avoidance capability. Moreover, for the aforementioned trajectory searching step, we provide two corresponding trajectory searching algorithms and discuss their feasibility. The contents and contribution of this paper are as follows.

- We apply trajectory searching methods to effectively generate restricted convex areas with the help of nominal trajectories, thereby mitigating non-convexity

while ensuring feasibility. Moreover, a customized artificial potential field method with kinematic reliability is proposed as a trajectory-searching algorithm. The customized artificial potential field approach may further be applied independently as a planning algorithm.

- Our proposed algorithms have been proven to produce trajectories with approximated optimal local minimal final time under specified conditions and moderate assumptions. Compared with general sequential-convex-programming-based motion planning solvers, the proposed method demonstrates superior robustness in dynamic environments and significantly reduces computational overhead, as evidenced by a higher success rate and lower total computation time in numerical experiments.
- By decomposing the complete problem into planning cycles and solving one planning cycle in parallel mode while moving, we have developed a robust framework that ensures both reliability and precision while only relying on a part of map information at a specific time.

In the remainder of this paper, the optimal control problem is formulated in Section II, providing a clear foundation for further analysis. In Section III, we introduce the two-layer model and develop trajectory searching algorithms, then thoroughly analyse them to demonstrate their effectiveness. Subsequent Section IV presents numerical experiments that utilize both static and dynamic maps, allowing us to present the conclusions in Section V.

2 Problem Formulation

In this section, we provide necessary annotations to ensure clarity and consistency throughout the paper. All the sets are discussed in Euclidean space \mathbb{R}^n with n specialized case by case and with the norm $\|\mathbf{a}\| = \sqrt{\langle \mathbf{a}, \mathbf{a} \rangle} = \sqrt{\mathbf{a}^\top \mathbf{a}}$, and we further let $\|\mathbf{a}\|_Q = \sqrt{\mathbf{a}^\top Q \mathbf{a}}$ with $Q \succ 0$. We also define sliced vectors, denoted by $\mathbf{a}[i : j]$, which consists of row i to row j from column \mathbf{a} . For instance, if $\mathbf{a} = [a_1, a_2, a_3, a_4]^\top$, then $\mathbf{a}[2 : 3] = [a_2, a_3]^\top$. For a differentiable function $f(\mathbf{x})$ with $\mathbf{x} \in \mathbb{R}^n$, we represent its gradient as $\nabla f(\mathbf{x})$, which is defined by $\left[\frac{\partial f}{\partial x_1}, \frac{\partial f}{\partial x_2}, \dots, \frac{\partial f}{\partial x_n} \right]^\top$. Moreover, the Euclidean norm of objects' velocity is referred to as speed in this paper.

2.1 Obstacle Avoidance Constraints

Generally, trajectory generation problems aim to provide feasible and safe trajectories for vehicles or other moving agents. In a trajectory generation problem, the vehicle is required to move in a specific space, which normally includes obstacles, a target state (or target area) and an initial state. This space is referred to as map, and we denote it by \mathcal{M} . Since each obstacle can be considered as a subset of \mathcal{M} , we can represent the spaces occupied by the i th obstacle as \mathcal{O}_i , with the relationship shown as

$$\mathcal{O}_i \subset \mathcal{M}, i \in \{1, 2, \dots, n_{obs}\} \quad (1)$$

with n_{obs} the number of obstacles. Without losing generality, we consider \mathcal{M} as an unbounded map. We further denote the occupied space by the vehicle as \mathcal{V} , then we have $\mathcal{V} \subset \mathcal{M}$. Throughout the entire task, no collision is allowed at any point in time. The corresponding constraints can be mathematically expressed as

$$\mathcal{O}_i \cap \mathcal{V} = \emptyset, \quad i \in \{1, 2, \dots, n_{obs}\}. \quad (2)$$

However, for irregularly shaped \mathcal{O}_i , it is difficult to analytically profile them, which poses a significant challenge in subsequent works. For simplicity, we apply

$$\mathcal{O}_i \subseteq \mathcal{B}(p_i, D_i/2) = \mathcal{B}_i \quad (3)$$

$i = 1, 2, \dots, n_{obs}$, and

$$\mathcal{V} \subseteq \mathcal{B}(x, D_v/2) = \mathcal{B}_v \quad (4)$$

as the approximated obstacles and vehicle, respectively. In (3) and (4), $\mathcal{B}(p, R)$ denotes a closed ball with the centre at p and the radius R . D_i and D_v are the diameter of the obstacles and vehicles, respectively, with the diameter of set A being

$$D_A = \begin{cases} 0 & A = \emptyset; \\ \sup\{y - x : x, y \in A, A \subseteq \mathcal{M}\} & \text{else.} \end{cases} \quad (5)$$

Thus, an approximated map can be created by substitute $\mathcal{O}_i, \mathcal{V}$ with $\mathcal{B}_i, \mathcal{B}_v$. In the approximated map, we do not need to consider the prior knowledge of the object shape, which greatly simplifies the design of subsequent algorithms. As a result, the obstacle avoidance constraints can be further represented as

$$\|x - p_i\| \geq \frac{D_i + D_v}{2} = r_i, \quad (6)$$

where $x = [x_1, x_2]^\top$ denotes the center position of \mathcal{B}_v . The shape approximation scheme relies on two critical assumptions which is given by Assumptions 1 and 2 below.

Assumption 1 *Given the map, the initial and target positions are excluded out of \mathcal{B}_i for $i \in \{1, 2, \dots, n_{obs}\}$.*

Assumption 2 *For any pair of indices i and j with $1 \leq i, j \leq n_{obs}$ and $i \neq j$, the spaces occupied by obstacles are disjoint. Moreover, it is assumed that there exists a positive constant ℓ with*

$$\mathcal{B}(p_i, r_i + 0.5\ell) \cap \mathcal{B}(p_j, r_j + 0.5\ell) = \emptyset,$$

for $i, j \in \{1, 2, \dots, n_{obs}\}$ and $i \neq j$.

Assumption 1 is critical because it establishes the feasible condition for tackling the original problem with the proposed algorithm. On the other hand, Assumption 2 presents a more permissive condition. This leniency can

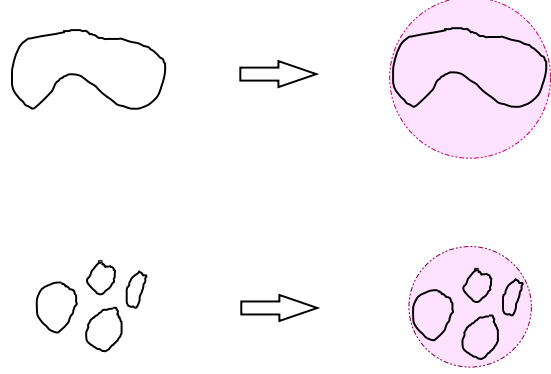


Fig. 1. A single irregular obstacle (top left) could be approximated as a closed ball (top right), while multiple dense small obstacles (bottom left) could merge into a single large one (top right pink circle) in consideration.

be interpreted by the fact that several small obstacles, along with their gaps, can be merged into a single large obstacle, as depicted in Fig.1. Therefore, it is evident that Assumption 2 is relatively mild.

2.2 Dynamics and Objective Function

We model the map and the dynamic equation in a unified Euclidean world coordinate system. In formulating the dynamic equation, we initially consider a linear model where the acceleration serves as the input. This consideration enables us to effectively depict the dynamic function in its most basic form as

$$\dot{z}(t) = A'z(t) + B'u(t) + w'(t), \quad (7)$$

where

$$A' = \begin{bmatrix} 0 & 0 & 1 & 0 \\ 0 & 0 & 0 & 1 \\ 0 & 0 & 0 & 0 \\ 0 & 0 & 0 & 0 \end{bmatrix},$$

$$B' = \begin{bmatrix} 0 & 0 & 1 & 0 \\ 0 & 0 & 0 & 1 \end{bmatrix}^\top$$

and $w'(t) = 0$. The state vector z is defined as the concatenation of the position vector x and its time derivation as $z = [x^\top, \dot{x}^\top]^\top$. If a nonlinear dynamic model is considered, for instance, the well-known Ackermann model, the corresponding dynamic function can be generally expressed as

$$\dot{z}(t) = \mathbf{F}(z, u, t).$$

In this nonlinear case, an approximated linear model with the same form as (7) can be obtained by calculating

the Jacobi matrix as

$$\begin{aligned} A' &= \frac{\partial \mathbf{F}}{\partial z} \Big|_{z=z'}, B' = \frac{\partial \mathbf{F}}{\partial u} \Big|_{u=u'}, \\ w' &= \mathbf{F} - \mathbf{F} \Big|_{z=z', u=u'}. \end{aligned} \quad (8)$$

Remark 1 It is well established that under most of the modelling frame, the dynamic equations are nonlinear. Although we can treat them as affine models by leveraging (8) as long as the dynamic functions are continuously differentiable, it loses precision and even results in generating fault solutions if the planning horizon considered is too long. Fortunately, we can treat the planning horizon as a “trust region”. In other words, the precision of the solution can be preserved if the linearized model is applied only in problems with small final times, which provides plausibility to the application of model linearization. Our algorithm only considers a limited horizon within each planning cycle, which enables us to handle nonlinear models in a correct manner.

The physical constraints of the vehicle can be represented as

$$0 \leq \|v(t)\| \leq v_{\max},$$

and

$$0 \leq \|\dot{x}(t)\| \leq a_{\max}.$$

These constraints can be further reformulated as $z^\top Q_1 z \leq 1$ and $u^\top Q_2 u \leq 1$. It is worth noting that although the probably max-speed of the vehicle is bounded by the motor’s power or other factors such as fraction, the scalar v_{\max} can be chosen under the value of the probably maximal speed for the consideration of safety. A lower v_{\max} tends to improve the successful rate, while a bigger v_{\max} ensures a smaller time cost.

Take z_0 and z_f as the initial and target state respectively, the boundary constraints can then be formulated as

$$z(0) = z_0, \quad (9)$$

$$\|z(t_f) - z_f\|_{Q_0} \leq \gamma, \quad (10)$$

where Q_0 is a positive definite weight matrix, t_f denotes the final time profiling the task’s time cost, $z(t_f)$ is the ending state and (10) profiles the target area.

Our main goal is to drive the vehicle to the target area with a possibly low time cost. Although this can be considered a time-optimal control problem, the task’s time cost is unnecessary to consider just yet. Instead, we adopt the cost function as

$$J = [z_f - z(t_f)]^\top Q_0 [z_f - z(t_f)]. \quad (11)$$

Under this model frame, the trajectory can meet (10) if a sufficient big t_f is given under Assumptions 1 & 2, and the continuous model is controllable.

2.3 Discretization and Transformation

Since it is not easy to solve continuous optimal control problems on computation devices, it is advised to convert the problem to discrete ones by shooting or other parameterization methods. In the discretization step, we substitute $z(t)$ by $\{z_1, z_2, \dots, z_{N+1}\}$ and $u(t)$ by $\{u_1, u_2, \dots, u_N\}$, then the constraints can be reformulated as

$$z_{i+1} - z_i = h_i (A' z_i + B' u_i + w'_i) \quad i = \{1, 2, \dots, N\}. \quad (12)$$

In (12), h_i represents the step lengths, which can be either constants or adapt to environmental changes. In this paper, we fixed the step length $h_i = h$ as a constant. Thus, it allows us to rewrite (12) to (13) as

$$z_{i+1} = Az_i + Bu_i + w_i, \quad (13)$$

while a necessary assumption is critical to further analysis that is presented in Assumption 3.

Assumption 3 In (13), (A, B) is controllable and B is of full column rank.

Similar to (13), two inequalities are formulated to represent discretized physical constraints, which can be represented as

$$G_1(z_i) = z_i^\top Q_1 z_i - 1 \leq 0, \quad (14)$$

$$G_2(u_i) = u_i^\top Q_2 u_i - 1 \leq 0. \quad (15)$$

The initial condition in the discretized problem can be reformulated as

$$z_1 = z_0, \quad (16)$$

while the converted boundary condition is

$$\|z_{N+1} - z_f\|_{Q_0} \leq \gamma. \quad (17)$$

The obstacle avoidance constraints can be further discretized as

$$\|z_i[1:2] - p_j\| \geq r_j \quad (18)$$

with $i \in \{1, 2, \dots, N+1\}$ and $j \in \{1, 2, \dots, n_{obs}\}$. Note that (18) is the sole non-convex constraint in the discretized problem, and serves as a key shorthand for general optimization-based motion planning controller operating in real-time tasks.

For the discretization of the cost function, we can rewrite (11) as

$$J = [z_f - z_{N+1}]^\top Q_0 [z_f - z_{N+1}]. \quad (19)$$

After all, given the time step h and problem size N , the discrete formulation of the planning problem can be represented as

$$\begin{aligned} \min & \quad (19), \\ \text{s.t.} & \quad (13) - (18), \end{aligned}$$

where we denote it by \mathcal{P}_1 . For the sake of convenience, if (17) is not considered in \mathcal{P}_1 , a relaxed version of \mathcal{P}_1 is then constructed, and we denote the relaxed problem by $\mathcal{P}'_1(z_0)$.

Remark 2 (12) and (13) use Euler method to approximate a derivation. Exactly, one can obtain a more precise approximation by setting

$$A = \exp(A'h),$$

$$B = \int_0^h \exp(A'\tau) d\tau \cdot B',$$

and

$$w_i = \int_0^h \exp(A'\tau) d\tau \cdot w'(ih).$$

Although various discretization methods can be applied, one critical property is that $z_{i+1} - z_i$ owns the same order as h . This property is vital in subsequent algorithm analysis.

3 Algorithm Analysis

Generally, problem \mathcal{P}_1 may be solved using nonlinear programming algorithms (NLP) or by convex optimization solvers iteratively via sequential convex programming (SCP). These approaches can be further categorized into one-shot and multi-step methods. The former involves solving a single problem to obtain the desired trajectory with tools like LCvx, whereas the latter entails iteratively calculating subproblems until the convergence is achieved. These methods are almost mature while predicting computation time and solution quality for general NLP solvers remain challenging due to some inherent difficulties in their basic algorithm. For instance, SCP is susceptible to artificial infeasibility, where the infeasibility arises from over-constrained subproblems. The SCP algorithms may also produce ill solutions if some subproblems are improperly constructed, highlighting the need for careful parameter tuning and initial reference trajectory selection. Compared with these general approaches, our method is too based on convex programming to guarantee low computational time. By synthesizing control inputs dynamically, an approximated time-optimal solution can be obtained although time-optimality is not considered in the cost function. Furthermore, our algorithm definitively solves the problem within stricter convexified constraint sets, guaranteeing the feasibility of the solution far more effectively than general SCP algorithms. In the rest of this section, we will propose our trajectory generation method with analysis. Firstly, two necessary alternated problems are formulated.

3.1 Unconstrained Problem

We denote $\mathcal{P}_w(z_0)$ as a relaxed version of $\mathcal{P}'_1(z_0)$, where (17) and all the non-convex obstacle avoiding constraints (18) are removed. Thus, $\mathcal{P}_w(z_0)$ can be constructed as

$$\min \quad (19),$$

$$\text{s. t. } (13) - (16).$$

Both the feasibility and the convexity of $\mathcal{P}_w(z_0)$ are ensured for given N and h since (17) is not considered in this problem. Consequently, we can solve this problem to obtain a nominal trajectory, which is presented as

$$S(\mathcal{P}_w) = \arg \min \mathcal{P}_w = \{\bar{z}_1, \dots, \bar{z}_{N+1}; \bar{u}_1, \dots, \bar{u}_N\}.$$

3.2 Strict Problem

The strict problems generate trajectories within more tightly constrained feasible sets, which grant the name. The formulation of the strict problem depends on a feasible trajectory and the nominal trajectory of $\mathcal{P}_w(\cdot)$. Suppose $F : \{\tilde{z}_1, \dots, \tilde{z}_{N+1}; \tilde{u}_1, \dots, \tilde{u}_N\}$ is aforementioned feasible trajectory of \mathcal{P}'_1 with $\tilde{z}_1 = \bar{z}_1 = z_0$. Since $\tilde{z}_i[1:2]$ are collision-free points, it is easy to find a vector $\lambda_{\min} = \{\lambda_{\min,1}, \lambda_{\min,2}, \dots, \lambda_{\min,N+1}\}$ with

$$\lambda_{\min,i} = \min \{ \max \{ \lambda_i : \exists p_j, r_j, \|z_i[1:2] - p_j\| = r_j \}, 0 \},$$

where $(\lambda \tilde{z}_i + (1 - \lambda) \tilde{z}_i)[1:2]$ are collision-free locations for any λ with $(0 < \lambda_{\min,i} < \lambda < 1)$. Furthermore, we can easily derive the fact that $[\lambda_{\min} \tilde{z} + (1 - \lambda_{\min}) \tilde{z}][1:2]$ lies on the edge of one obstacle near to F . Thus, some convex sets can be extracted from the original problem by

$$\begin{aligned} \mathcal{Z}_i = \{ z_c | z_c = & (1 - \lambda_{\min,i} + \lambda_{f,i} - \lambda_{\min,i} \lambda_{f,i}) \tilde{z}_i \\ & + (\lambda_{\min,i} + \lambda_{f,i} - \lambda_{\min,i} \lambda_{f,i} - \lambda_{d,i}) \tilde{z}_i \\ & + \lambda_{d,i} \tilde{z}_{i-1}, 0 \leq \lambda_{d,i} \leq \lambda_{f,i} \leq 1 \}, \end{aligned} \quad (20)$$

for $i = \{2, 3, \dots, N+1\}$. The above sets profile a triangle area in the map. Specifically, to maintain the consistency, define

$$\begin{aligned} \mathcal{Z}_1 = \{ z_c | z_c = & (1 - \lambda_{\min,1} + \lambda_{f,1} - \lambda_{\min,1} \lambda_{f,1}) \tilde{z}_1 \\ & + (\lambda_{\min,1} + \lambda_{f,1} - \lambda_{\min,1} \lambda_{f,1} - \lambda_{d,1}) \tilde{z}_1 \\ & + \lambda_{d,1} \tilde{z}_1, 0 \leq \lambda_{d,1} \leq \lambda_{f,1} \leq 1 \}. \end{aligned} \quad (21)$$

Although the convexity of these extracted sets are guaranteed, the non-feasibility may remain. To further ensure the feasibility, linear inequality constraints on $\lambda_{f,i}, \lambda_{d,i}$ are introduced as

$$\lambda_{d,i} \leq k_i \lambda_{f,i}. \quad (22)$$

(22), k_i are pre-selected to keep the convexified area out of obstacles. We denote the strict problem as $\mathcal{P}_s(z_0)$, which can be presented as

$$\min_{\{\lambda_f, \lambda_d\}} J_s(\lambda_f, \lambda_d; \rho) = J(z(\lambda_f, \lambda_d), u(\lambda_f, \lambda_d))$$

$$+ \rho \cdot \|z_0 - z_f\| \|\lambda_f - \mathbf{1}\|^2, \quad (23)$$

$$\text{s.t. } 0 \leq \lambda_{f,i} \leq 1, \quad (24)$$

$$(13), (14), (15), (16), (22).$$

In (23), we denote $\lambda_f = (\lambda_{f,1}, \lambda_{f,2}, \dots, \lambda_{f,N+1})^\top$, $\lambda_d = (\lambda_{d,1}, \lambda_{d,2}, \dots, \lambda_{d,N+1})^\top$. Moreover, note that (22) and (24) are equivalent reformulation of

$$z_i[1 : 2] \in \mathcal{Z}_i[1 : 2]. \quad (25)$$

Although \mathcal{P}_s is feasible, its solution generally violates (17) since a small planning horizon is given to guarantee precision and reliability. To handle this difficulty, our algorithm solves \mathcal{P}_s iteratively with planning cycles and dynamically updating relative parameters to get out of this dilemma. This manner also maintains the quality of the trajectory. Algorithm 1 uses pseudo code to depict the strategy of our proposed two-layer programming model. Throughout the entire planning process, some specific challenges may arise, which we define as connective infeasibility as Definition 1 represents.

Definition 1 *During the planning process, if an extreme z_{N+1} is obtained, i.e. $z_{N+1}[1 : 2]$ locates very close to an obstacle, and it tends to move ahead of the obstacle with a high speed, infeasibility may arise in the subsequent planning cycle. This phenomenon is referred to as connective infeasibility.*

To mitigate the connective infeasibility, $\rho \|\lambda_f - \mathbf{1}\|$ is introduced in $\mathcal{P}_s(z_0)$ to enhance the robustness where it is referred to as the safety term.

Algorithm 1 Online Programming Algorithm

```

1: Input: The map information  $\mathcal{M}$ .
2:  $K \leftarrow 1$ ;
3: while  $\|z_{N^{(K)}+1} - z_f\|_{Q_0} \geq \gamma$  do
4:   Get Current State  $z_0^{(K)}$ 
5:   Get a Collision Free Trajectory  $F^{(K)} : \{z_1, \dots, z_{N^{(K)}+1}; u_1, \dots, u_{N^{(K)}}\}^{(K)}$ 
6:   Generate Problem  $\mathcal{P}_w^{(K)}(z_0^{(K)})$ 
7:   Get  $S(\mathcal{P}_w^{(K)}(z_0^{(K)}))$ 
8:   Solve Problem  $\mathcal{P}_s^{(K)}(z_0^{(K)}) \rightarrow \{u_1^{(K)}, \dots, u_{N^{(K)}}^{(K)}\}$ 
9:   if  $\|z_{N^{(K)}+1} - z_f\|_{Q_0} \geq \gamma$  then
10:    Adjust  $N^{(K)}$  to  $\hat{N}^{(K)}$  with  $\hat{N}^{(K)} < N^{(K)} - 1$ 
       and  $\hat{N}^{(K)} \leq N_{\max}$ 
11:   end if
12:   Apply  $\{u_1, \dots, u_{\hat{N}^{(K)}}\}$ 
13:   Update  $\rho^{(K)}, A, B, w, z_0$ 
14:    $K \leftarrow K + 1$ 
15: end while

```

In Algorithm 1, we use $(\cdot)^{(K)}$ to represent relative parameters in the K^{th} planning cycle, and the steps to get $F^{(K)}$ are referred to as searching algorithm. At the beginning of Algorithm 1, Q_0 and an initial state are pro-

vided. The algorithm generates a trajectory comprised of $N^{(1)}$ grids of control signals by solving the first cycle. Subsequently, the vehicle moves to the position $z_{\hat{N}^{(1)}+1}^{(1)}$ using the generated control signal. Concurrently, another planning cycle is constructed utilizing $z_{\hat{N}^{(1)}+1}^{(1)}$ as the predicted initial state $z_0^{(2)}$ and an renewed $\rho^{(2)}$ as the coefficient of the safety term. This iterative process continues until the quit condition (17) is reached. In this process, although all the problems are formulated as final time-fixed, we can obtain free final time solutions by synthesizing control inputs from each planning cycle sequentially. Note $N^{(K)}$ are initially generated from searching algorithms correspondingly, subsequently they are used as the problem size in both $\mathcal{P}_w^{(K)}$ and $\mathcal{P}_s^{(K)}$. For the sake of safety and quality, the solution of one planning cycle is applied only partially by choosing a smaller $\hat{N}^{(K)}$ and applying $\{u_1, \dots, u_{\hat{N}^{(K)}}\}$, where we will show its significance in analysis.

Up to this point, we have established the main framework of our planning algorithm. Before proceeding with the algorithm analysis, we will first present two customized trajectory searching algorithms which demonstrate good performance in experiments.

3.3 Customized Vortex Artificial Potential Field

The APF method [26] simulates a virtual force field to guide a robot towards its goal while avoiding obstacles. The approach is inspired by the way physical systems behave under conservative forces such as gravity and tension. This dynamic-equation-ignored planning method is almost perfect while fragile in complex environments. Based on APF, the VAPF algorithm provides a more sophisticated framework employed in robotics and autonomous systems for navigation and path planning. Utilizing concepts from general potential field methods, VAPF extends the potential field by incorporating vortex-like behaviours, which modulate the repulsive force into a vortex pattern, and introduce a rotational field that can help to navigate through complex environments instead of adding purely radial influence from obstacles. As the normal VAPF suggests, the attractive potential is constructed by the square of l_2 -norm, which is defined as

$$P_{att}(z[1 : 2]) = \|z[1 : 2] - z_f[1 : 2]\|^2. \quad (26)$$

The repulsive potential acts to drive the vehicle away from obstacles, where we formulate it with the form similar to [27] as

$$P_{rep}(z[1 : 2]) = \zeta \sum_{j=1}^{n_{obs}} \exp \left(\frac{-\beta \cdot (\|x - p_j\| - r_j)}{r_j} \right). \quad (27)$$

If a standard APF algorithm is considered, the moving direction can be obtained instantly by calculating $-(\nabla P_{att} + \nabla P_{rep})$ directly. For the vortex field which

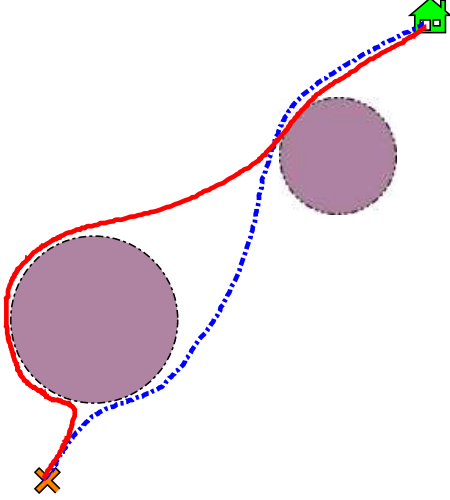


Fig. 2. The solid red line and the dashed blue line represent two possible paths on a map. However, sharp turns in the red path typically signal that the vehicle is slowing down at those points, leading to longer travel times and lower solution quality.

denoted by E_v , it is normally vertical to P_{rep} , which follows

$$\begin{cases} \mathbf{d} \in \mathcal{D} : \left\{ \tilde{\mathbf{d}} \in \text{Null}(\nabla P_{rep}(z[1:2])) \mid \|\tilde{\mathbf{d}}\| = 1 \right\} \\ E_v(z[1:2]) = \zeta_v(\mathbf{d}); \end{cases}$$

here, $\text{Null}(\cdot)$ represents the null space, \mathbf{d} is the direction of the vortex field and ζ_v is the scale of the vortex force. In a 2-D map, \mathcal{D} includes at least two elements. Moreover, if $\nabla P_{rep} = 0$, \mathbf{d} can be a unit vector with an arbitrary direction. Adding an extra direction selecting criterion could help the VAPF algorithm to generate quality paths. For instance, it could help to find a shorter way when avoiding an obstacle in the forward of the vehicle, as shown in Fig.2. Denote the expected subsequent moving direction of point \tilde{z}_i as $E_{\tilde{z}_i}^\dagger$, then the direction can be obtained by calculating

$$E_{\tilde{z}_i} = -(\nabla P_{att}(\tilde{z}_i[1:2]) + \nabla P_{rep}(\tilde{z}_i[1:2])) + E_v(\tilde{z}_i[1:2]),$$

and

$$E_{\tilde{z}_i}^\dagger = \frac{E_{\tilde{z}_i}}{\|E_{\tilde{z}_i}\|_2}.$$

The introduction of the vortex field also brings other benefits, for instance, it helps to generate smoother trajectories which are less prone to oscillations. The vortex field also reduces the likelihood of local minima traps that generally appear in APF, allowing for more fluid and natural movement through crowded or complex spaces. However, it is worth noting that these paths may be implementable since they may fail to meet the dynamic constraint. In order to overcome this hurdle, we

have designed the Customized Vortex Artificial Potential Field (CVAPF) by introducing an extra speed search step. Once the expected moving direction at the current point is determined, the reachable speed towards the expected moving direction will be calculated instantly according to the physical constraints. If achievable speeds exist, the subsequent velocity will then be determined by collaborating the moving direction and a reliable speed. If there exists no speed which meets the constraint combined with the expected moving direction, a safety acceleration will then be applied to slow down the vehicle and divert it toward the expected moving direction simultaneously. The pseudo-code of our proposed CVAPF is demonstrated as Algorithm 2. In Algorithm 2, a_{safe}

Algorithm 2 Customized VAPF Algorithm

```

1: Input: Map Information  $\mathcal{M}$ , Current state  $z_0^{(K)}$ .
2:  $N \leftarrow 0$ ;
    $\tilde{z}_0 \leftarrow z_0^{(K)}$ ;
3: while  $((N < N_{\min} \text{ or } \text{NotSafe}) \text{ and } N \leq N_{\max})$  do
4:    $\tilde{z}_{N+1} = \tilde{z}_N[1:2] + \tilde{z}_N[3:4] \cdot \Delta t$ 
5:   Calculate  $E(\tilde{z}_{N+1}), E^\dagger(\tilde{z}_{N+1})$ 
6:   Search a speed  $s_{N+1}$  from  $v_{\max} \rightarrow 0$  which meets
   the constraints with the moving direction
7:   if Search is successful then
8:      $\tilde{z}_{N+1}[3:4] = s_{N+1}E^\dagger(\tilde{z}_{N+1})$ 
9:   else
10:     $a_{safe} = [a_1 E^\dagger(\tilde{z}_{N+1}) - a_0 \frac{\tilde{z}_N[3:4]}{\|\tilde{z}_N[3:4]\|}]$ 
11:     $\tilde{z}_{N+1}[3:4] = \tilde{z}_N[3:4] + a_{safe} \cdot \Delta t$ 
12:   end if
13:   Update  $\zeta_v$ 
14:   Update Not_Safe
15:    $N \leftarrow N + 1$ 
16: end while
17: if Not_Safe = 1 then
18:   Algorithm Failed;
19: else
20:   Calculate  $\{\tilde{u}_1, \tilde{u}_2, \dots\}$ 
21:   Return Feasible Trajectory  $F^{(K)}$ 
22:   Return  $N^{(K)} \leftarrow N$ 
23: end if

```

is utilized to lower the speed of the vehicle and alter its direction. Since

$$\begin{aligned} \|a_{safe}\| &= \left\| a_1 E^\dagger(\tilde{z}_{i+1}) - a_0 \frac{\tilde{z}_i[3:4]}{\|\tilde{z}_i[3:4]\|} \right\|, \\ &\leq \|a_1 E^\dagger(\tilde{z}_{i+1})\| + \left\| a_0 \frac{\tilde{z}_i[3:4]}{\|\tilde{z}_i[3:4]\|} \right\|, \\ &= a_1 + a_0, \end{aligned}$$

$a_{safe} \leq a_{\max}$ can be easily guaranteed by selecting a_1 and a_0 with $a_0 + a_1 \leq a_{\max}$.

The choice of N also plays a significant role in generating quality trajectories. During our experiments, we have found that it can enhance robustness by having the

trajectory searching algorithm terminate at a safer position. For instance, connective infeasibility can greatly be mitigated. This observed phenomenon motivate us to introduce a `Not_Safe` signal accordingly. The update rule for `Not_Safe` can be described as follows:

$$\text{Not_Safe} = \begin{cases} 0, & T_s = \emptyset, \\ 1, & \text{else,} \end{cases}$$

where

$$T_s = \left\{ t \in [0, t_w] \mid z_{N+1}[1 : 2] + z_{N+1}[3 : 4]t \in \bigcup_{i=1}^{n_{obs}} \mathcal{B}_i \right\}.$$

At the same time, $\min T_s$ is a vital parameter used in the updating of $\rho^{(K)}$, where a smaller $\min T_s$ requires bigger $\rho^{(K)}$. Since $N^{(K)}$ generated in Algorithm 2 can be large, adjusting $N^{(K)}$ is meaningful to maintain the precision. These steps also show the necessity to substitute $N^{(K)}$ with $\hat{N}^{(K)}$ in Algorithm 1. Simultaneously, N_{\max} is further introduced to confine the length of applied control input in one planning cycle.

3.4 Customized Dynamic Window Approach

Dynamic Window Approach (DWA) [28] is another kind of seminal algorithm in mobile robotics, which is also renowned for its efficacy in real-time path planning and navigation. By judiciously balancing the trade-offs between speed and safety, DWA enables agents to navigate dynamic environments with minimal risks. The main principle of DWA is exactly the “dynamic window”, which is the set of feasible control inputs an agent can operate at its current states taking into account factors such as position, orientation, speed, and constraints. From the view of the agent, it is critical to predict how it can take action in its current state, which is to construct the dynamic window. From the perspective of the algorithm designer, a policy to decide the action in these sets is paramount to consider.

In order to apply DWA effectively in our scenario, we further develop the Customized Dynamic Window Approach (CDWA) algorithm. Following the general DWA methods, we first identify the dynamic window at the current state, which is achieved by calculating the possible control inputs based on constraints. Next, a subset of these feasible inputs is extracted for evaluation according to the map information, `Not_Safe` flag and $\min T_s$. The state of the next time step is instantly anticipated using the chosen input while refreshing the current state by the anticipated state in the end. Repeat these processes several loops to ultimately generate a trajectory consisting of N inputs and $N+1$ states. The pseudo-code of our proposed CDWA is demonstrated in Algorithm 3. Up to this point, two customized trajectory search algorithms have been provided. We will subsequently show the convergence property of Algorithm 1 in a mild assumption given in Assumption 4.

Algorithm 3 Customized DWA Searching Algorithm

```

1: Input: Map information  $\mathcal{M}$ , state  $z_0$ .
2:  $N \leftarrow 1$ ;
3: while  $((N < N_{\min} \text{ or } \text{NotSafe}) \text{ and } N \leq N_{\max})$ 
   do
4:   Detect Obstacles along the direction of current
   velocity
5:   Calculate the dynamic window
6:   Obtain  $\min\{T_s\}$ 
7:   Obtain current acceleration
8:   Update notsafe
9:    $N \leftarrow N + 1$ 
10: end while
11: Do step 15-21 in Algorithm 2

```

Assumption 4 For all planning cycles, there exists $0 \leq \kappa < 1$, which makes

$$J_s(z^{(K)}, u^{(K)}) \leq \kappa J_s(z^{(K-1)}, u^{(K-1)}) \quad (28)$$

hold for almost every K . In other words, the number of cycles which violate (28) is limited.

To explain the reasonableness of Assumption 4, we can divide the circumstances into two cases. For the Case I, consider that $J_s^{(K-1)} \gg \gamma$. Under this precondition, the cost from velocity can be set to a relatively small level if a Q_0 is chosen properly, and the cost function is then mainly decided by the position. Thus, $J_s^{(K+1)} \leq J_s^{(K)}$ is naturally satisfied with the assistance of the searching algorithm if the initial velocity $z_0^{(K)}[3 : 4]$ remains moderate. On the other hand, if the initial velocity is undesirable, e.g. the vehicle moves away from the target area at maximum speed, it can still achieve (28) after several cycles. Moreover, when encountering obstacles, the vehicle necessitates strategic decision-making regarding its directional maneuver. Since all the obstacles are circle-like, there exists at least one direction that makes the vehicle gets closer to the target area. The search algorithm can prioritize this direction. Experiments also show the mildness of Case I. Case II is complementary to Case I. When $J_s^{(K-1)} \gg \gamma$ is not satisfied, properly readjusting $\rho^{(K)}$ can drive the vehicle to meet the boundary constraint according to the convexity property of \mathcal{P}_s if the trajectory searching algorithm can divert the vehicle to the target area. Thus, Assumption 4 is moderate. Combined with Assumption 1, it can be proven that the target area is reachable within limited planning cycles, as demonstrated in Theorem 1.

Theorem 1 For given γ , $z_{N+1}^{(K+1)}$ can be obtained with $\|z_{N+1}^{(K+1)} - z_f\|_{Q_0} \leq \gamma$ after executing finite planning cycles.

Proof. Under Assumption 4, we only need to suppose (28) is violated at the planning cycle K_1, K_2, \dots, K_m .

Moreover, we define

$$\kappa_i = \frac{J_s(\lambda_f^{(K_i+1)}, \lambda_d^{(K_i+1)}; \rho^{(K_i+1)})}{J_s(\lambda_f^{(K_i)}, \lambda_d^{(K_i)}; \rho^{(K_i)})}. \quad (29)$$

We can deduct that $K_m + 1$ cannot be the last iteration. Then, for any $K \geq K_m$, it has

$$\prod_{i=1}^K \frac{J_s(\lambda_f^{(i+1)}, \lambda_d^{(i+1)}; \rho^{(i+1)})}{J_s(\lambda_f^{(i)}, \lambda_d^{(i)}; \rho^{(i)})} \leq \kappa^{K-m} \cdot \prod_{i=1}^m \kappa_i. \quad (30)$$

During each planning cycle except the last one, $\|z_{N+1}^{(K+1)} - z_f\| \geq \gamma$ keeps true. As a result, $J_s(\lambda_f^{(K)}, \lambda_d^{(K)}; \rho^{(K)}) \geq \gamma$ is consistently satisfied, which indicates that $\kappa_i \leq J_s(\lambda_f^{(K_i+1)}, \lambda_d^{(K_i+1)}; \rho^{(K_i+1)})/\gamma$ are too bounded for any κ_i . Consequently, we have

$$\begin{aligned} \|z_{N+1}^{(K+1)} - z_f\| &\leq J_s(\lambda_f^{(K+1)}, \lambda_d^{(K+1)}, \rho^{(K+1)}) \\ &\leq \kappa^{K-m} \cdot \prod_{i=1}^m \kappa_i \cdot J_s(\lambda_f^{(1)}, \lambda_d^{(1)}, \rho^{(1)}). \end{aligned} \quad (31)$$

Taking

$$K > \frac{\left(\log \gamma - \log J_s(\lambda_f^{(1)}, \lambda_d^{(1)}, \rho^{(1)}) - \sum_{i=1}^m \log \kappa_i \right)}{\log \kappa} + m, \quad (32)$$

we can then guarantee $\|z_{N^{(K)}+1}^{(K+1)} - z_f\|_{Q_0} \leq \gamma$ after executing K planning cycles, thereby complete the proof. \square

Theorem 1 provides conclusive evidence that Algorithm 1 terminates with finite planning cycles under the given assumptions, therefore it is guaranteed that Algorithm 1 generates “practical” trajectories. Building upon this foundation, our subsequent work aims to establish a sufficient condition for the local optimality property of the synthesized trajectory.

Theorem 2 Suppose A, B keep unchanged during each cycle. Given an initial state $z_1, \{u_1, u_2, \dots, u_m\}$ is an m -grids local optimal solution of $\mathcal{P}'_1(z_1)$, and $\{u'_{m'+1}, \dots, u_{m+n}\}$ is a local optimal solution of $\mathcal{P}'_1(z_{m'+1})$ at the initial state $z_{m'+1}$ with n -grids, where $1 < m' \leq m - 1$. Note that $u'_{m'}$ is applied to distinct with $u_{m'}$ in the solution of $\mathcal{P}'_1(z_1)$. Then, $\{u_1, u_2, \dots, u_m; u'_{m'+1}, \dots, u_{m+n}\}$ is a local optimal solution of $\mathcal{P}'_1(z_1)$ with $m' + n$ grids, if $u_{m'}^\top Q_2 u_{m'} < 1$. Note that $\{u'_{m'+1}, \dots, u_{m+n}\}$ is extracted from $\mathcal{P}'_1(z_{m'+1})$.

Proof. When A, B are time-invariant in each cycle, suppose $\{z_1, z_2, \dots, z_{m'}, z_{m'+1}, \dots, z_{m'+n+1}\}$ is obtained under the synthesized control input. We can formulate the Lagrangian function of $\mathcal{P}'_1(z_1)$ with $m' + n$

state grids as follows:

$$\begin{aligned} L_{m'+n} &= \|z_{m'+n}\|_{Q_0}^2 + \sum_{i=1}^{m'+n} v_i (z_{i+1} - Az_i - Bu_i - w_i) \\ &+ \sum_{i=1}^{m'+n+1} \sum_{j=1}^{N_{obs}} \zeta_{ij} (r_j^2 - \|z_i[1:2] - p_j\|^2) \\ &+ \sum_{i=1}^{m'+n+1} s_i G_1(z_i) + \sum_{i=1}^{m'+n} q_i G_2(u_i). \end{aligned} \quad (33)$$

Similarly, we can form the Lagrangian function of two separate problems as L_m and L_n . Noting that for i with $i \notin \{1, m'+1, m'+n+1\}$, it could obtain

$$\begin{aligned} \frac{\partial L_{m'+n}}{\partial z_i} &= \frac{\partial}{\partial z_i} \sum_{j=1}^{N_{obs}} \zeta_{ij} (r_j^2 - \|z_i[1:2] - p_j\|^2) \\ &- A^\top v_i + v_{i-1} + 2s_i Q_1 z_i, \end{aligned} \quad (34)$$

and

$$\frac{\partial L_{m'+n}}{\partial u_i} = -B^\top v_i + 2q_i Q_2 u_i, \quad (35)$$

which are also the partial derivation of L_m or L_n with respect to z_i and u_i , respectively. While for $z_{m'+1}$ we have

$$\begin{aligned} \frac{\partial L_m}{\partial z_{m'+1}} &= \frac{\partial}{\partial z_{m'+1}} \sum_{j=1}^{N_{obs}} \zeta_{m'+1,j} (r_j^2 - \|z_{m'+1}[1:2] - p_j\|^2) \\ &- A^\top v_{m'+1} + v_{m'} + 2s_{m'+1} Q_1 z_{m'+1}. \end{aligned}$$

If $u_{m'}$ is in the interior of the input constraint, then by the complementary slackness property, we have

$$\frac{\partial L_m}{\partial u_{m'}} = -B^\top v_{m'} = \mathbf{0}.$$

Since B is of full column rank, we can obtain that $v_{m'} = \mathbf{0}$. On the other hand, for L_n , we have

$$\begin{aligned} \frac{\partial L_n}{\partial z_{m'+1}} &= A^\top v_{m'+1} + 2s_{m'+1} Q_1 z_{m'+1} \\ &+ \frac{\partial}{\partial z_{m'+1}} \sum_{j=1}^{N_{obs}} 2\zeta_{m'+1,j} (r_j^2 - \|z_{m'+1}[1:2] - p_j\|^2). \end{aligned} \quad (36)$$

If $L_{m'+n}$ reaches the optimality, all the variables and multipliers of the synthesized trajectory must lie in the optimal set of L_m and L_n simultaneously. Thus, we have

$$\frac{\partial L_n}{\partial z_{m'+1}} = \frac{\partial L_m}{\partial z_{m'+1}} \Rightarrow A^\top v_{m'+1} = A^\top v_{m'+1} + v_{m'}. \quad (37)$$

This equation could be ensured by $v_{m'} = \mathbf{0}$. Note that all other first-order optimality conditions of $L_{m'+n}$ can be guaranteed respectively by the KKT condition of $L_{m'}$ and L_n . Therefore, we can conclude the proof. \square

Remark 3 In Theorem 2, the local optimal property is with respect to $\mathcal{P}'_1(\cdot)$. Exactly, if (17) is further satisfied in the synthesized solution, it is easy to deduct that the solution is also local optimality in \mathcal{P}_1 .

Analog to the proof of Theorem 2, we can further obtain a stronger conclusion, which is demonstrated in Corollary 1.

Corollary 1 Suppose that A, B are time-varying matrices between iterations, and we denote them as

$$\{A_1, \dots, A_{m'}, A'_{m'+1}, \dots, A_{m'+n}\}$$

and

$$\{B_1, \dots, B_{m'}, B'_{m'+1}, \dots, B_{m'+n}\}.$$

Then, Theorem 2 keeps validity under the following two conditions if $m' \leq m - 2$ and

- 1). $u_m^\top Q_2 u_{m'} < 1$, $u_{m'+1}^\top Q_2 u_{m'+1} < 1$ and $u_{m'+1}^\top Q_2 u_{m'+1} < 1$ hold simultaneously;
- 2). $B_{m'}, B_{m'+1}$ and $B'_{m'+1}$ are of full column rank.

Theorem 2 and Corollary 1 reveal the soundness of synthesis segmented control inputs and further illuminate the rule of adjusting $N^{(K)}$. Although we only considered patching 2 segments in Theorem 2, it is easy to extend the conclusion to multiple trajectory synthesis cases. Moreover, in some specific cases, the aforementioned trajectory synthesizing method can reliably identify the global optimal trajectory, even when dealing with non-convex constraint sets. This result is formally established in Theorem 3.

Theorem 3 Among the planning cycles, if $\lambda_{\min,i}^{(K)} = 0$ holds for $i = 1, 2, \dots, N^{(K)}$ with $K = 1, 2, \dots$, and the conditions in Theorem 2 are satisfied, then

$$\{u_1^{(1)}, \dots, u_{\hat{N}^{(1)}}^{(1)}; u_1^{(2)}, \dots, u_{\hat{N}^{(2)}}^{(2)}; \dots; u_1^{(K)}, \dots, u_{N^{(K)}}^{(K)}\}$$

in Theorem 2 globally solves $\mathcal{P}'_1(z_1)$.

Proof. Let us start by constructing a relaxed problem $\mathcal{P}'_2(z_0)$ as

$$\begin{aligned} \min \quad & (z_{N^{(K)}+1}^{(K)} - z_f)^\top Q_0 (z_{N^{(K)}+1}^{(K)} - z_f), \\ \text{s. t.} \quad & (13) - (16). \end{aligned}$$

By Theorem 2, $\{z_1^{(1)}, \dots, z_{N^{(K)}+1}^{(K)}\}$ is a local optimal trajectory of $\mathcal{P}'_1(z_1^{(1)})$. Note that if $\lambda_{\min,i}^{(K)} \equiv 0$, $i = 1, 2, \dots, N^{(K)}$ with $K = 1, 2, \dots$, the whole trajectories are then unaffected by any of the non-convex obstacles. For the K th planning cycle, its solution is optimal of $\mathcal{P}_w^{(K)}(\cdot)$; hence we can conclude that $\{z_1^{(1)}, \dots, z_{N^{(K)}+1}^{(K)}\}$

is also a local optimal solution of $\mathcal{P}'_2(z_1^{(1)})$. With the convexity of $\mathcal{P}'_2(\cdot)$, it can further prove the global optimality of $\{z_1^{(1)}, \dots, z_{N^{(K)}+1}^{(K)}\}$. Using the fact that the global optimal solution of $\mathcal{P}'_2(\cdot)$ has a lower or equal cost to the global optimal solution of $\mathcal{P}'_1(\cdot)$, it can obtain that $\{z_1^{(1)}, \dots, z_{N^{(K)}+1}^{(K)}\}$ is also a global optimal trajectory of $\mathcal{P}'_1^{(1)}$, which completes the proof. \square

The aforementioned theorems have shown the main principle of trajectory synthesizing, establishing that it is possible to find a available control input for navigating our vehicle by solving optimization problems sequentially and synthesizing segment solutions. Furthermore, we have proved that in specific cases, global optimality can be achieved.

In the subsequent discussion, we will delve into another critical index: the travelling time cost. This metric provides insight into how quickly the vehicle can arrive at the target area from its initial state, offering a crucial evaluation of Algorithm 1's purpose. Generally, various free final time optimization methods can be employed to address time-optimal control problems. Given our discretization is based on fixed step lengths, Algorithm 1 utilizes $\hat{N}^{(K)}$ from its planning cycles to profile time cost. In fact, we can obtain the final time as

$$t_f = h \sum_{i=1}^{K-1} \hat{N}^{(i)} + h \hat{N}^{(K)}.$$

Since $h \hat{N}^{(K)} \leq h N_{\max}$, one can obtain a preciser evaluation of t_f by using a smaller horizon $N_{\max}h$. However, it is unnecessary to calculate an accurate t_f to present the “fastness” of the trajectory. Instead, we could demonstrate that t_f is achieved approximately to a local minimal final time. To show this claim, suppose that $\{z_1^{(j)}, \dots, z_{\hat{N}^{(K)}+1}^{(j)}\}$ are extracted from solving $\mathcal{P}'_1^{(1)}(z_0^{(1)}), \mathcal{P}'_1^{(2)}(z_0^{(2)}), \dots, \mathcal{P}'_1^{(K)}(z_0^{(K)})$, and that the solution of $\mathcal{P}'_1^{(K)}(z_0^{(K)})$ satisfies the quit condition of Algorithm 1; then, we have $\hat{N}^{(K)} = N^{(K)}$. If $\{u_1^{(1)}, \dots, u_{N^{(K)}+1}^{(K)}\}$ is a local optimal solution of \mathcal{P}_1 , then there exists δ , and for arbitrary $\{u_1^{(1)}(\delta), \dots, u_{N^{(K)}+1}^{(K)}(\delta)\}$ satisfying all of the constraints, we have

$$(z_{N^{(K)}+1}^{(K)}(\delta) - z_f)^\top Q_0 (z_{N^{(K)}+1}^{(K)}(\delta) - z_f) \geq \gamma^2 \geq J^{(K)};$$

here, we denote $z_{(\cdot)}^{(\cdot)}(\delta)$ as the state obtained by using the control serial $\{u_1^{(1)}(\delta), \dots, u_{N+1}^{(K)}(\delta)\}$. If $(z_{N^{(K)}+1}^{(K)}(\delta) - z_f)^\top Q_0 (z_{N^{(K)}+1}^{(K)}(\delta) - z_f) \geq \gamma^2$, Algorithm 1 will continue with at least one planning cycle. In this circumstance, suppose $U(\delta) = \{u_1^{(1)}(\delta), \dots, u_{N+1}^{(K)}(\delta), \dots\}$ is a

feasible solution of \mathcal{P}_1 , then it can be obtained that

$$t_f(\delta) - t_f \geq h$$

with $t_f(\delta)$ the final time of using $U(\delta)$. Otherwise, if $(z_{N^{(K)}+1}^{(K)}(\delta) - z_f)^\top Q_0(z_{N^{(K)}+1}^{(K)}(\delta) - z_f) \leq \gamma^2$, then we have $t_f(\delta) = t_f$. The tendency toward local optimal solutions becomes more pronounced with shorter time horizons. To show this, we rewrite the quit condition to an equivalent form as

$$\|z_{N^{(K)}+1}^{(K)} - z_f\|_{Q_0}^2 \leq \gamma^2. \quad (38)$$

Then, we have

$$\|z_{N^{(K)}+1}^{(K)} - z_f\|_{Q_0}^2 - \|z_{N^{(K)}+1}^{(K-1)} - z_f\|_{Q_0}^2 \quad (39)$$

$$\leq 2\|z_1^{(1)} - z_f\| \|z_{N^{(K)}+1}^{(K)} - z_{N^{(K)}+1}^{(K-1)}\| \|Q_0\|_2 \quad (40)$$

$$\leq 2\|z_1^{(1)} - z_f\| \cdot (\|z_{N^{(K)}+1}^{(K)} - z_{N^{(K-1)}+1}^{(K-1)}\| \\ + \|z_{N^{(K-1)}+1}^{(K-1)} - z_{N^{(K-1)}+1}^{(K-1)}\|) \cdot \|Q_0\|_2. \quad (41)$$

For $\|z_{N^{(K)}+1}^{(K)} - z_{N^{(K-1)}+1}^{(K-1)}\|$, we can further obtain

$$\begin{aligned} & \|z_{N^{(K)}+1}^{(K)} - z_{N^{(K-1)}+1}^{(K-1)}\| \\ &= \|z_{N^{(K)}+1}^{(K)} - z_1^{(K)}\| \\ &\leq \sum_{i=1}^{N^{(K)}} \|z_{i+1}^{(K)} - z_i^{(K)}\| \\ &= h \cdot \sum_{i=1}^N \|A' z_i^{(K)} + B' u_i^{(K)} + w_i^{(K)}\| \\ &\leq N_{\max} h \cdot \max_{i=1, \dots, N} \left\{ \|A' z_i^{(K)} + B' u_i^{(K)} + w_i^{(K)}\| \right\}. \end{aligned} \quad (42)$$

Similarly, we have

$$\begin{aligned} & \|z_{N^{(K-1)}+1}^{(K-1)} - z_{N^{(K-1)}+1}^{(K-1)}\| \\ &\leq \sum_{i=\hat{N}^{(K-1)}+1}^{N^{(K-1)}} \|z_{i+1}^{(K-1)} - z_i^{(K-1)}\| \\ &\leq N_{\max} h \\ &\quad \cdot \max \left\{ \|A' z_i^{(K-1)} + B' u_i^{(K-1)} + w_i^{(K-1)}\| \right\}. \end{aligned} \quad (43)$$

In the above steps, (40) is a direct result of Assumption 4. With the boundness of $u_i^{(K)}$ and $z_i^{(K)}$, (41), (42) and (43) indicate (39) $\rightarrow 0$ as $N_{\max} h \rightarrow 0$. With $\|z_{N^{(K-1)}+1}^{(K-1)} - z_f\|_{Q_0} > \gamma$ and $\|z_{N^{(K)}+1}^{(K)} - z_f\|_{Q_0} \leq \gamma$,

we can obtain $\|z_{N^{(K)}+1}^{(K)} - z_f\|_{Q_0} \rightarrow \gamma^-$ as $N_{\max} h \rightarrow 0$. This means that we can choose a sufficient small $N_{\max} h$, that making all $\{u_1^{(1)}(\delta), \dots, u_{N+1}^{(K)}(\delta)\}$ failed to meet the quit condition for given δ except $\{u_1^{(1)}, \dots, u_{N+1}^{(K)}\}$ itself. Thus, $h \sum_{i=1}^K \hat{N}^{(i)}$ converges to a local minimal t_f .

Remark 4 Although $h \sum_{i=1}^K \hat{N}^{(i)}$ converges to a local minimum as $N_{\max} h \rightarrow 0$, some undesired phenomenons may appear if $N_{\max} h$ is too small, e.g. the conditions of Theorem 2 may be difficult to be satisfied. Therefore, t_f can generally approximate to a local minimal final time since a lower bound of $N_{\max} h$ should be added.

Next, some sufficient conditions for the equivalence between $\mathcal{P}_s(z_0^{(K)})$ and $\mathcal{P}'_1(z_0^{(K)})$ will be provided. We begin with defining the relative interior solution.

Definition 2 For $\mathcal{P}_s^{(K)}$, a feasible solution is defined as a relative interior solution, if all the elements $z_i^{(K)}[1 : 2]$ for $i = 1, \dots, N^{(K)} + 1$ lie within the relative interior of $\mathcal{Z}_i[1 : 2]$.

Theorem 4 When $\rho^{(K)} = 0$, a control serial calculated from the optimal solution of $\mathcal{P}_s^{(K)}(z_0^{(K)})$ is a local optimal control for $\mathcal{P}'_1(z_0^{(K)})$, if at least one of the following two cases is satisfied.

1). All $\lambda_{\min, i}^{(K)} = 0$ or $\tilde{z}_i = \bar{z}_i$, $i \in \{1, \dots, N^{(K)} + 1\}$.

2). The obtained optimizer of $\mathcal{P}_s^{(K)}$ is a relative interior solution.

Proof. See Appendix A. \square

Up to this point, we have discussed some properties of Algorithm 1 without the considerations of safety term by setting $\rho^{(j)} = 0$ in $\mathcal{P}_s^{(j)}(\cdot)$. Next, we will briefly introduce how the safety term affects the solution. Suppose $\{\lambda_f^*(\rho), \lambda_d^*(\rho)\}$ is an optimal solution of $\mathcal{P}_s(z_0^{(K)})$ with $\rho^{(K)} = \rho$. Then, we can obtain

$$\begin{aligned} & J(z^{(K)}(\lambda_f^*(0), \lambda_d^*(0)), u^{(K)}(\lambda_f^*(0), \lambda_d^*(0))) \\ &+ 0 \cdot \|z_0^{(K)} - z_f\| \|\lambda_f^*(0) - \mathbf{1}\|^2 \\ &\leq J(z^{(K)}(\lambda_f^*(\rho), \lambda_d^*(\rho)), u^{(K)}(\lambda_f^*(\rho), \lambda_d^*(\rho))) \\ &+ \rho \cdot \|z_0^{(K)} - z_f\| \|\lambda_f^*(\rho) - \mathbf{1}\|^2 \\ &\leq J(z^{(K)}(\lambda_f^*(0), \lambda_d^*(0)), u^{(K)}(\lambda_f^*(0), \lambda_d^*(0))) \\ &+ \rho \cdot \|z_0^{(K)} - z_f\| \|\lambda_f^*(0) - \mathbf{1}\|^2 \\ &\leq J(z^{(K)}(\lambda_f^*(0), \lambda_d^*(0)), u^{(K)}(\lambda_f^*(0), \lambda_d^*(0))) \\ &+ \rho N_{\max} \|z_0^{(K)} - z_f\|. \end{aligned} \quad (44)$$

To analyze the trajectory error from the introduction of the safety term, we need to present two important theorems first, which are demonstrated as Theorem 5 and Theorem 6, respectively.

Theorem 5 Suppose $f(\mathbf{x})$ is a continuous closed convex function defined in $\mathbf{x} \in \mathbb{E} \subset \mathbb{R}^{l_f}$ and the minimum of f is denoted by f_{\min} . Define $\Phi_f(s) = D_{\text{Lev}}(f, s)$ which is

a mapping of $\Phi_f : [f_{opt}, \infty) \rightarrow [0, \Phi_f(\infty))$, then $\Phi_f(s)$ is upper semi-continuous for $s \in [f_{opt}, \infty)$ provided that $f(\mathbf{x})$ has only one minimizer in \mathbb{E} . Here,

$$\text{Lev}(f, s) = \{\mathbf{x} : f(\mathbf{x}) < s\}$$

is the strict level set of f at s , and

$$\overline{\text{Lev}}(f, s) = \{\mathbf{x} : f(\mathbf{x}) \leq s\}$$

is the level set of f at s .

Proof. See Appendix B. \square

Theorem 5 is based on the condition that the optimizer of f is unique. If this condition is not satisfied, it can also easily obtain that $\Phi_f(s)$ is upper semi-continuous for $s \in (f_{opt}, \infty)$ while its upper semi-continuous range changes to $[\overline{\text{Lev}}(f, f_{opt}), \infty)$. Using similar mathematical method, we can further prove another important theorem, which is presented as Theorem 6.

Theorem 6 Suppose X^* is the optimal set of f with $f(\mathbf{x}^*) = f_{opt}$ for any $\mathbf{x}^* \in X^*$. If X^* is bounded, then

$$\varphi(s) = \begin{cases} \max_{\mathbf{x} \in \text{Lev}(f, s)} \{\|\text{Proj}_{X^*}(\mathbf{x}) - \mathbf{x}\|\}, & f_{opt} < s, \\ 0, & \text{else} \end{cases}$$

is upper semi-continuous for $s \in [f_{opt}, \infty)$, and

$$\lim_{s \rightarrow f_{opt}^+} \left(\max_{\mathbf{x} \in \text{cl}(\text{Lev}(f, s))} \|\mathbf{x} - \text{Proj}(\mathbf{x})\| \right) = 0. \quad (45)$$

Proof. See Appendix C. \square

Since \mathcal{P}_s is convex, combining (44) we can obtain that as $\rho/\|Q\|_2 \rightarrow 0^+$ the difference between $\{\lambda_f^*(\rho), \lambda_d^*(\rho)\}$ and $\{\lambda_f^*(0), \lambda_d^*(0)\}$ converges to 0 according to the conclusion of Theorem 6. As a result, it is reasonable to consider the solution of $\mathcal{P}_s(\cdot)$ as the optimal solution of $\mathcal{P}_1'(\cdot)$ while ignoring the effect of the safety term, if $\|Q_0\|_2 \gg \rho$ and any of the two cases in Theorem 4 is satisfied.

Despite the aforementioned strict problems can be solved with lower computational burdens, their local optimality condition is not as moderate as initially thought. If a stricter local optimal solution is required, SCP can also be an effective substitution for searching algorithms, That is to use SCP algorithm to get a local optimal solution for each planning cycle. Applying SCP to the two-layer programming model also yields numerous benefits, surpassing the trajectory obtained by directly applying SCP to the original problem. In particular, when both SCP methods have a comparable number of nodes, Algorithm 1 exhibits even greater advantages still due to its reduced computational requirements. This is because Algorithm 1 is only required to calculate a limited set of future trajectory parameters in one cycle, resulting in lower computation power and increased reliability. However, these short-sighted trajectories may arise connective infeasibility while general SCP algorithms do not.

Theoretically, the computation complexity and time-optimality of the aforementioned algorithms are drafty tabulated in TABLE I.

Table 1
A Rough Comparison Between Algorithms

	Calculating Time	t_f
SCP	+++	+
Two-layer model + Searching	+	++
Two-layer model + SCP	++	+

In this table, more “+” represents larger indexes. Although our analysis only guarantees the time optimality for limited scenarios, empirical experiments reveal that the two-layer algorithm excels at generating efficient control inputs with a relatively lower t_f and a fast computation speed. More detailed comparisons are given in the next section by numerical experiments.

4 Numerical Experiments

In this section, some numerical experiments are presented to illustrate the capabilities of Algorithm 1 in both static and time-varied map scenarios. We conduct these experiments using MATLAB 2017a with the assistance of the CVX toolbox.

4.1 Experiments with Static Maps

In this part, we generate maps with fixed circular obstacles to evaluate the algorithm’s capability in static scenarios. The critical characteristics of interest can be depicted as vehicle parameters and map parameters, which are presented in Table 2.

Table 2
Parameters

Vehicle Parameters	v_{\max}	a_{\max}	z_f	$z_0^{(1)}$
Range	15	20	$[160, 160, 0, 0]^\top$	$0_{4 \times 1}$
Map parameters	n_{obs}	r_i	ℓ	γ
Range	20	$[3, 11]$	7	3

In the process of map generation, the circle obstacles are created and distributed stochastic by built-in random functions, a check step is then used to verify whether the target point is reachable and the map parameters are satisfied. To show the vehicle’s performance to the reader, we choose one map and run simulations respectively with Algorithm 1 and its competition algorithms. The simulated trajectories is visualized in Fig.3.

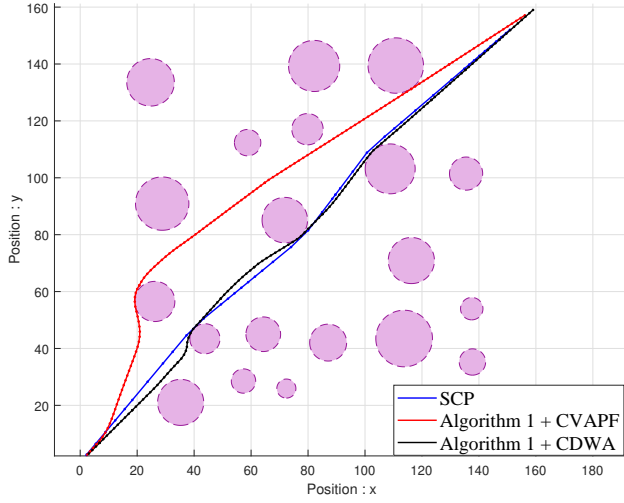


Fig. 3. Trajectories generated by 3 distinct algorithm

In Fig.3, the red line represents the trajectory obtained using our two-layer optimization model with the CVAPF searching algorithm, the black line corresponds to the result from Algorithm 1 while utilizing CDWA to get $F^{(K)}$. In contrast, the blue line depicts the trajectory obtained by a general sequential convex programming algorithm, which is parameterized with 45 nodes. Notably, all the three trajectories are feasible yet exhibit varying qualities of performance. To facilitate a detailed comparison, we have conducted experiments to measure both the final time and Relative Calculating Time (RCT), as listed in TABLE III.

Table 3
Quality Comparison

	SCP(45 nodes)	SCP(20 nodes)	CVAPF	CDWA
t_f (seconds)	24.64	19.3	16.44	15.72
RCT(%)	100*	61.4	34.9	36.9

Correspondingly, the control inputs are shown in Fig.4. In the three charts, the red dashed line represents the acceleration of the x -direction, while the blue dashed line represents the acceleration of the y -direction.

To further evaluate the capability of Algorithm 1, we employ various metrics in subsequent experiments. Specifically, we utilize indexes such as t_f , successful rate, and computational time to assess performance. We first test the computation time. In this part, each algorithm is individually tested on 100 maps, with results plotted in Fig. 5 and statistical indicators listed in TABLE IV, where we use SCP45 and SCP20 are the abbreviations of Sequential Convex Programming with 45 Nodes and Sequential Convex Programming with 20 Nodes respectively.

In TABLE 4, We could further see more details of these experiments, which include various metrics for evaluat-

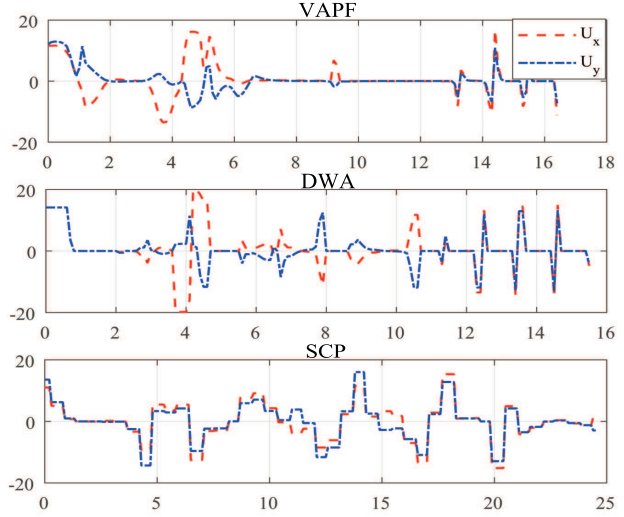


Fig. 4. The inputs generated by distinct algorithms: (1) Algorithm 1 with CVAPF, (2) Algorithm 1 with CDWA, and (3) a direct SCP-based approach with 45 nodes.

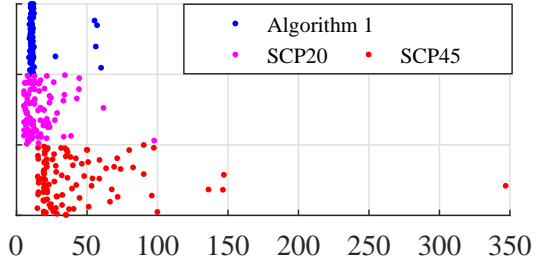


Fig. 5. A comparison of the running time between SCPs and our algorithm

Table 4
Quality Comparison of Distinct Algorithms

	SCP45	SCP20	Algorithm 1 + CDWA
Success Rate(%)	90.4	60.2	91.1
RCT(Average)	255.2	100*	74.74
RCT(Worst)	355.2	100*	35.74
RCT(Medium)	220.9	100*	85.11

ing the performance of our two-layer optimization algorithm, e.g. averaged relative calculating time, worst relative calculating time and the median. Fig.5 further provides insight into the reliability and predictability of our planning model by highlighting the computation time of Algorithm 1 and its competition methods. Notably, it reveals that our two-layer optimization model outper-

forms SCP algorithms in terms of calculation efficiency, with a shorter average computing time while having a more concentrated distribution of results. In contrast, SCP algorithms exhibit longer computation times and a more scattered distribution, and this is particularly evident as the number of nodes increases. Moreover, it can be observed that each dataset contains significantly larger samples than anticipated. Since our two-layer algorithm requires generating new trajectories before the vehicle reaches the end of its last control sequence, trials with abnormal computation time should be considered as failed experiments and are excluded from successful rate calculations. Despite this limitation, experiment data suggests that Algorithm 1 performs better than a general SCP method in certain static map scenarios.

4.2 Experiments with Dynamic Maps

In this part, we will conduct experiments to show the robustness of Algorithm 1 in time-varying maps with moving obstacles. Firstly, we revise and add some extra parameters shown in Table 5 to profile a time-varying map.

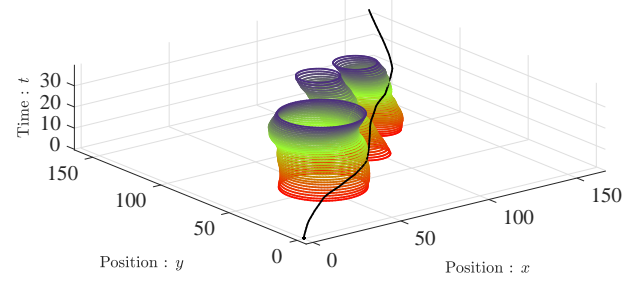
Table 5

The Parameters included in the experiments with time-varying maps

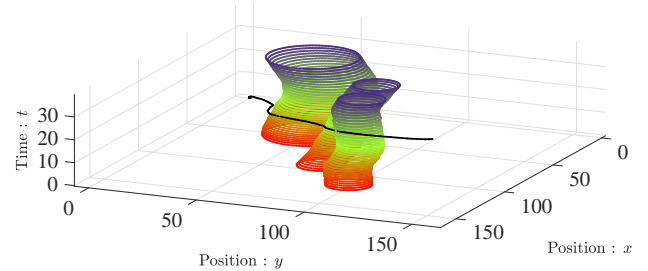
Vehicle Parameters	v_{\max}	a_{\max}	z_f	$z_0^{(1)}$
Range	6.0	6.0	$[160, 160, 0, 0]^T$	$0_{4 \times 1}$
Map parameters	n	r_i	ϵ	v_o
Range	$\{3, 20\}$	$[3, 11]$	7	$0.3v_{\max}$

Here, v_o is applied to depict the maximal speed of obstacles, where for arbitrary $p_i(t)$ there exists $\|p_i(t + \tilde{t}) - p_i(t)\| \leq v_o \cdot |\tilde{t}|$ for any t and \tilde{t} . For demonstration purposes, we initially set the number of obstacles to 3 in a toy example since using a map with fewer obstacles allows for a clear and concise illustration of the algorithm's behaviour in figures. Then, as part of its validation process, we also test Algorithm 1 with a larger dynamic scenario featuring 20 moved obstacles. To make the motion simulation of the obstacle more realistic, we determine the position of the obstacle by using a double integrator with saturation. In other words, for each simulation step, an obstacle's velocity is detected at the first. Then, analogue to the DWA, a dynamic acceleration set which meets the subsequent velocity is constructed. The acceleration is randomly selected in these sets instantly. After determining the acceleration, its velocity and position are updated sequentially by numerical integration. In the example, two figures are plotted to show the specific movement of the vehicle and obstacles in two distinct perspectives, which are demonstrated in Fig. 6.

In Fig.6, both graphs share the same vertical axis, representing the time. When the vertical coordinates are specified, the corresponding horizontal plane represents



(a) Perspective 1



(b) Perspective 2

Fig. 6. Obstacle avoidance experiment in time-varied scenarios: A Result

the danger areas from obstacles at that particular moment. The solid black line indicates the vehicle's trajectory throughout the task. By combining these two charts, it becomes evident that Algorithm 1 effectively avoids obstacles, showcasing its capability with the assistance of searching algorithms in a dynamic map. Furthermore, to aid readers in comprehending the obstacle avoidance capabilities of the vehicle more clearly, we provide a corresponding display diagram as depicted in Fig.7.

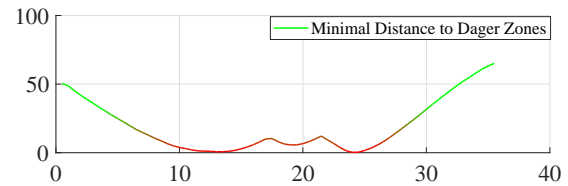


Fig. 7. The minimal distance to danger zones during the task. in this figure, the minimal value is 0.2760

In Fig.7, the minimal distance between the vehicle and

danger zones is demonstrated. It shows that the vehicle keeps a distance bigger than 0.2760m from all the danger zones at any time.

With $n = 20$, we conduct subsequent experiments, testing Algorithm 1 with 150 diverse maps. The results are demonstrated in TABLE 6.

Table 6
Quality Comparison in Time Varying maps

	Successful Rate%	RCT(Average)	RCT(medium)
CVAPF	94.6	93.75	95.71
CDWA	93.3	100*	100*

Next, we will experimentally demonstrate the impact of v_{\max} on the performance of Algorithm 1. In this part, we set v_{\max} as an independent variable and maintain all other parameters constant. To comprehensively evaluate its effects, we test Algorithm 1 with a large number of randomly created maps, each with distinct v_{\max} . The results are presented in TABLE 7.

Table 7
Reliability under Different v_{\max}

v_{\max} (m/s)	5.0	7.0	9.0	14.0
Successful Rate(%)	87.0	87.5	82.6	76.6

Our previous assertion is supported by this result, which suggests that a smaller v_{\max} tends to yield more flexible steering and improves reliability. In contrast, setting v_{\max} to larger value results in a potential of decreased reliability while the benefit is the reduction of t_f .

5 Conclusion

Our two-layer optimization-based planning algorithm demonstrated its capability in both theoretical proof and numerical experiments. Specifically, when v_{\max} is well selected, the two-layer planning model outperforms general sequential convex programming algorithms, achieving an optimal balance between time optimality and reliability. However, the model still encounters challenges in extreme scenarios. One key limitation arises from its discrete solution generation, which only guarantees the feasibility in given discrete time points. As a result, it may struggle with feasibility at interpolated states, which is also a common issue faced by general motion planning algorithms. When the planning horizon for a single cycle is excessively long, the timeliness of solutions is compromised, and the algorithm may fail in dynamic scenarios where obstacles continue to shift. Additionally, the computation time for a single planning cycle may exceed the horizon of the latest generated control sequences, potentially leading to loss of vehicle control. To address these

shortcomings of Algorithm 1, our future works will focus on enhancing robustness through more reliable searching methods and conducting a detailed analysis of non-linear vehicle models.

References

- [1] Brian Paden, Michal Čáp, Sze Zheng Yong, Dmitry Yershov, and Emilio Frazzoli. A survey of motion planning and control techniques for self-driving urban vehicles. *IEEE Transactions on Intelligent Vehicles*, 1(1):33–55, 2016.
- [2] Peter E. Hart, Nils J. Nilsson, and Bertram Raphael. A formal basis for the heuristic determination of minimum cost paths. *IEEE Transactions on Systems Science and Cybernetics*, 4(2):100–107, 1968.
- [3] Xiang Liu and Daoxiong Gong. A comparative study of a-star algorithms for search and rescue in perfect maze. In *2011 International Conference on Electric Information and Control Engineering*, pages 24–27, 2011.
- [4] Tao Zheng, Yanqiang Xu, and Da Zheng. Agv path planning based on improved a-star algorithm. In *2019 IEEE 3rd Advanced Information Management, Communicates, Electronic and Automation Control Conference (IMCEC)*, pages 1534–1538, 2019.
- [5] Gang Tang, Congqiang Tang, Christophe Claramunt, Xiong Hu, and Peipei Zhou. Geometric a-star algorithm: An improved a-star algorithm for agv path planning in a port environment. *IEEE Access*, 9:59196–59210, 2021.
- [6] Zhi Lin, Kang Wu, Rulin Shen, Xin Yu, and Shiquan Huang. An efficient and accurate a-star algorithm for autonomous vehicle path planning. *IEEE Transactions on Vehicular Technology*, 73(6):9003–9008, 2024.
- [7] Baichuan Liu, Weikun Zhang, Wuhui Chen, Huawei Huang, and Song Guo. Online computation offloading and traffic routing for uav swarms in edge-cloud computing. *IEEE Transactions on Vehicular Technology*, 69(8):8777–8791, 2020.
- [8] A. Stentz. Optimal and efficient path planning for partially-known environments. In *Proceedings of the 1994 IEEE International Conference on Robotics and Automation*, pages 3310–3317 vol.4, 1994.
- [9] Maxim Likhachev, Geoffrey Gordon, and Sebastian Thrun. Ara*: Anytime a* with provable bounds on sub-optimality. volume 16, 01 2003.
- [10] J.J. Kuffner and S.M. LaValle. Rrt-connect: An efficient approach to single-query path planning. In *Proceedings 2000 ICRA. Millennium Conference. IEEE International Conference on Robotics and Automation. Symposia Proceedings (Cat. No.00CH37065)*, volume 2, pages 995–1001 vol.2, 2000.
- [11] Yoshiaki Kuwata, Justin Teo, Gaston Fiore, Sertac Karaman, Emilio Frazzoli, and Jonathan P. How. Real-time motion planning with applications to autonomous urban driving. *IEEE Transactions on Control Systems Technology*, 17(5):1105–1118, 2009.
- [12] Sertac Karaman, Matthew R. Walter, Alejandro Perez, Emilio Frazzoli, and Seth Teller. Anytime motion planning using the rrt*. In *2011 IEEE International Conference on Robotics and Automation*, pages 1478–1483, 2011.
- [13] Alejandro Perez, Robert Platt, George Konidaris, Leslie Kaelbling, and Tomas Lozano-Perez. Lqr-rrt*: Optimal sampling-based motion planning with automatically derived extension heuristics. In *2012 IEEE International Conference on Robotics and Automation*, pages 2537–2542, 2012.

- [14] Reza Mashayekhi, Mohd Yamani Idna Idris, Mohammad Hossein Anisi, Ismail Ahmedy, and Ihsan Ali. Informed rrt*-connect: An asymptotically optimal single-query path planning method. *IEEE Access*, 8:19842–19852, 2020.
- [15] Namwook Kim, Sukwon Cha, and Huei Peng. Optimal control of hybrid electric vehicles based on pontryagin’s minimum principle. *IEEE Transactions on Control Systems Technology*, 19(5):1279–1287, 2011.
- [16] Gao Tang, Fanghua Jiang, and Junfeng Li. Fuel-optimal low-thrust trajectory optimization using indirect method and successive convex programming. *IEEE Transactions on Aerospace and Electronic Systems*, 54(4):2053–2066, 2018.
- [17] F. Yegenoglu, A.M. Erkmen, and H.E. Stephanou. Online path planning under uncertainty. In *Proceedings of the 27th IEEE Conference on Decision and Control*, pages 1075–1079 vol.2, 1988.
- [18] Behcet Acikmese and Scott R. Ploen. Convex programming approach to powered descent guidance for mars landing. *Journal of Guidance, Control, and Dynamics*, 30(5):1353–1366, 2007.
- [19] John M. Carson, Behcet Acikmese, and Lars Blackmore. Lossless convexification of powered-descent guidance with non-convex thrust bound and pointing constraints. In *Proceedings of the 2011 American Control Conference*, pages 2651–2656, 2011.
- [20] Behcet Acikmese, John M. Carson, and Lars Blackmore. Lossless convexification of nonconvex control bound and pointing constraints of the soft landing optimal control problem. *IEEE Transactions on Control Systems Technology*, 21(6):2104–2113, 2013.
- [21] Federico Augugliaro, Angela P. Schoellig, and Raffaello D’Andrea. Generation of collision-free trajectories for a quadrocopter fleet: A sequential convex programming approach. In *2012 IEEE/RSJ International Conference on Intelligent Robots and Systems*, pages 1917–1922, 2012.
- [22] Danylo Malyuta, Taylor P. Reynolds, Michael Szmuk, Thomas Lew, Riccardo Bonalli, Marco Pavone, and Behcet Acikmese. Convex optimization for trajectory generation: A tutorial on generating dynamically feasible trajectories reliably and efficiently. *IEEE Control Systems Magazine*, 42(5):40–113, 2022.
- [23] Riccardo Bonalli, Abhishek Cauligi, Andrew Bylard, and Marco Pavone. Gusto: Guaranteed sequential trajectory optimization via sequential convex programming. In *2019 International Conference on Robotics and Automation (ICRA)*, pages 6741–6747, 2019.
- [24] Lars Blackmore, Behcet Acikmese, and John M. Carson. Lossless convexification of control constraints for a class of nonlinear optimal control problems. In *2012 American Control Conference (ACC)*, pages 5519–5525, 2012.
- [25] Patrick Scheffe, Theodor Mario Henneken, Maximilian Kloock, and Bassam Alrifae. Sequential convex programming methods for real-time optimal trajectory planning in autonomous vehicle racing. In *2024 IEEE Intelligent Vehicles Symposium (IV)*, pages 3144–3144, 2024.
- [26] O. Khatib. Real-time obstacle avoidance for manipulators and mobile robots. In *Proceedings. 1985 IEEE International Conference on Robotics and Automation*, volume 2, pages 500–505, 1985.
- [27] Yan Gao, Dazhi Li, Zhen Sui, and Yantao Tian. Trajectory planning and tracking control of autonomous vehicles based on improved artificial potential field. *IEEE Transactions on Vehicular Technology*, 73(9):12468–12483, 2024.

- [28] D. Fox, W. Burgard, and S. Thrun. The dynamic window approach to collision avoidance. *IEEE Robotics & Automation Magazine*, 4(1):23–33, 1997.

A Proof of Theorem 4

For simplicity, the indicator of iteration order are omitted, e.g. $z^{(K)} \rightarrow z$. Take $\rho = 0$. Recall the Lagrange function of $\mathcal{P}_s(z_0)$ can be formulated as $L(z_0; z, u, v, \zeta, s, q)$ with the same form of (33). If $L(z_0; z^*, u^*, v^*, \zeta^*, s^*, q^*)$ is a local minimum of L , then it holds following KKT conditions:

$$\left\{ \begin{array}{l} Az_i^* + Bu_i^* - z_{i+1}^* = \mathbf{0}, \\ s_i^* G_1(z_i^*) = \mathbf{0}, \\ q_i^* G_2(u_i^*) = \mathbf{0}, \\ \zeta_{ij}^* \left(r_j^2 - \|z_i^*[1:2] - p_j\|^2 \right) = \mathbf{0}, \\ s_i^* \geq 0, q_i^* \geq 0, \zeta_{ij}^* \geq 0, \\ z_1^* = z_0 \end{array} \right.$$

and

$$\{z_i^*, u_i^*\} = \arg \min_{z_i, u_i} L. \quad (\text{A.1})$$

Our goal is to demonstrate that the solution of $\mathcal{P}_s(z_0)$ satisfies the above KKT conditions. Take

$$L' = L - \sum_{i=1}^{N+1} \sum_{j=1}^{n_{obs}} \zeta_{ij} \left(r_j^2 - \|z_i[1:2] - p_j\|^2 \right).$$

Then, for the strict problem, the following optimal conditions can be derived as

$$\begin{aligned} L_s(z_0; z, u, v, \eta, \sigma, \xi, s, q) &= L' \\ &+ \sum_{i=1}^{N+1} (\eta_i - \sigma_i) \lambda_{f,i} - \eta_i + \sum_{i=1}^{N+1} \xi_i (\lambda_{d,i} - k_i \lambda_{f,i}). \end{aligned} \quad (\text{A.2})$$

If $\lambda_{\min,i} = 0$ holds for arbitrary i , then the nominal trajectory itself is feasible, which is also a minimizer of L . Otherwise, if a relative interior solution is obtained, we have

$$\zeta_{ij}^* = \eta_i^* = \sigma_i^* = \xi_i^* = 0$$

for all i by complement slackness condition. Actually, now we can obtain that $L_s \equiv L$. The first order optimality conditions of the strict problem are

$$\left\{ \begin{array}{l} \frac{\partial L_s}{\partial \lambda_{f,i}^*} = 0, \\ \frac{\partial L_s}{\partial \lambda_{f,d}^*} = 0 \end{array} \right. \quad (\text{A.3})$$

or

$$\{\lambda_{f,i}^*, \lambda_{d,i}^*\} = \arg \min_{\lambda_{f,i}, \lambda_{d,i}} L_s. \quad (\text{A.4})$$

In $\mathcal{P}_s(\cdot)$, it is worth noting that one pair of $\{\lambda_{f,i}, \lambda_{d,i}\}$ determines $\{z_i\}$ uniquely. Moreover, since

$$Bu_i = z_{i+1} - Az_i - w_i \quad (\text{A.5})$$

and B is of full column rank, we can derive that a given $\{\lambda_{f,i}, \lambda_{d,i}\}$ determines a unique state with unique input. In other words, (A.4) is a sufficient condition of (A.1). Thereby, we complete the proof. \square

B Proof of Theorem 5

It is easy to obtain two properties of Φ_f : (i), since the minimizer of Φ is a singleton, we have $\Phi_f(f_{opt}) = \Phi_f(f_{opt}^+) = 0$; (ii), for $s_1 \geq s_2 \geq f_{opt}$, we have $\Phi_f(s_1) \geq \Phi_f(s_2) \geq 0$.

Suppose Φ is not upper semi-continuous at $\tilde{s} > f_{opt}$. Then, leverage the monotonic non-decrease property of Φ_f , for any given $\delta > 0$, there exists an $\epsilon > 0$ with

$$\Phi_f(\tilde{s} + \delta) - \Phi_f(\tilde{s}) \geq \epsilon. \quad (\text{B.1})$$

Suppose $\mathbf{x}(\tilde{s}), \mathbf{y}(\tilde{s})$ are one pair of the cluster points of $\text{Lev}(f, \tilde{s})$ where their distance reaches $D(\text{Lev}(f, \tilde{s}))$. Then, with (B.1) we can derive

$$\begin{aligned} \Phi_f(\tilde{s} + \delta) - \Phi_f(\tilde{s}) &= \|\mathbf{x}(\tilde{s} + \delta) - \mathbf{y}(\tilde{s} + \delta)\| \\ &\quad - \|\mathbf{x}(\tilde{s}) - \mathbf{y}(\tilde{s})\| \\ &\leq \|\mathbf{x}(\tilde{s} + \delta) - \mathbf{x}(\tilde{s})\| \\ &\quad + \|\mathbf{y}(\tilde{s} + \delta) - \mathbf{y}(\tilde{s})\|. \end{aligned} \quad (\text{B.2})$$

Thus, we have

$$\|\mathbf{x}(\tilde{s} + \delta) - \mathbf{x}(\tilde{s})\| + \|\mathbf{y}(\tilde{s} + \delta) - \mathbf{y}(\tilde{s})\| \geq \epsilon. \quad (\text{B.3})$$

Since (B.3) holds for arbitrary $\{\mathbf{x}(\tilde{s} + \delta), \mathbf{y}(\tilde{s} + \delta)\} \subset \text{cl}(D(\text{Lev}(f, \tilde{s} + \delta)))$ with $\|\mathbf{x}(\tilde{s} + \delta) - \mathbf{y}(\tilde{s} + \delta)\| = \Phi_f(\tilde{s} + \delta)$, we can further obtain

$$\begin{aligned} \epsilon &\leq \min_{\mathbf{x}(\tilde{s} + \delta), \mathbf{y}(\tilde{s} + \delta)} \{\|\mathbf{x}(\tilde{s} + \delta) - \mathbf{x}(\tilde{s})\| \\ &\quad + \|\mathbf{y}(\tilde{s} + \delta) - \mathbf{y}(\tilde{s})\|\}. \end{aligned} \quad (\text{B.4})$$

Utilize the fact that all the strict level sets are open, we can derive $\mathbf{x}(\tilde{s}), \mathbf{y}(\tilde{s})$ lie on the boundary of $\text{cl}(\text{Lev}(f, \tilde{s}))$ with $f(\mathbf{x}(\tilde{s})) = f(\mathbf{y}(\tilde{s})) = \tilde{s}$. Then, by choosing a non-increasing series $\{\delta_n\}$ which converges to 0, we have

$$\begin{aligned} &\left(\lim_{\delta \rightarrow 0^+} \text{Lev}(f, \tilde{s} + \delta) \right) \setminus \text{Lev}(f, \tilde{s}) \\ &= \left(\lim_{n \rightarrow \infty} \bigcap_{i=1}^n \text{Lev}(f, \tilde{s} + \delta_i) \right) \setminus \text{Lev}(f, \tilde{s}) \\ &= \overline{\text{Lev}}(f, \tilde{s}) \setminus \text{Lev}(f, \tilde{s}) \end{aligned}$$

$$= \{\mathbf{x} : f(\mathbf{x}) = \tilde{s}\}. \quad (\text{B.5})$$

By (B.4), at least one inequality of

$$\begin{cases} \|\mathbf{x}(\tilde{s} + \delta) - \mathbf{x}(\tilde{s})\| \geq \epsilon/2, \\ \|\mathbf{y}(\tilde{s} + \delta) - \mathbf{y}(\tilde{s})\| \geq \epsilon/2 \end{cases}$$

holds as $\delta \rightarrow 0^+$, which indicates that at least one of $\mathbf{x}(\tilde{s} + \delta)$ or $\mathbf{y}(\tilde{s} + \delta)$ is out of $\text{cl}(\text{Lev}(f, \tilde{s}))$ (Note that the fact holds since once $\mathbf{x}(\tilde{s} + \delta), \mathbf{y}(\tilde{s} + \delta) \in \text{cl}(\text{Lev}(f, \tilde{s}))$, (B.1) and (B.4) cannot be satisfied simultaneously). Hence, suppose $\|\mathbf{x}(\tilde{s} + \delta) - \mathbf{x}(\tilde{s})\| \geq \epsilon/2$ as $\delta \rightarrow 0^+$, we can find a \mathbf{x}^\dagger with $\mathbf{x}^\dagger \notin \text{cl}(\text{Lev}(f, \tilde{s}))$, $\mathbf{x}^\dagger \in (\text{Lev}(f, \tilde{s}) \cup \{\mathbf{x} : f(\mathbf{x}) = \tilde{s}\}) \setminus \text{Lev}(f, \tilde{s})$. Note

$$\overline{\text{Lev}}(f, \tilde{s}) = \left(\lim_{n \rightarrow \infty} \bigcap_{i=1}^n \text{Lev}(f, \tilde{s} + \delta_i) \right),$$

which preserves the convexity of $\overline{\text{Lev}}(f, \tilde{s})$. Moreover, we have

$$\begin{aligned} &\text{conv}(\text{Lev}(f, \tilde{s}), \mathbf{x}^\dagger) \setminus \text{Lev}(f, \tilde{s}) \\ &\subset \overline{\text{Lev}}(f, \tilde{s}) \setminus \text{Lev}(f, \tilde{s}) \\ &= \{\mathbf{x} : f(\mathbf{x}) = \tilde{s}\}. \end{aligned} \quad (\text{B.6})$$

By (B.6), there exists interior points in $\{\mathbf{x} : f(\mathbf{x}) = \tilde{s}\}$. Take $\mathbf{x}^* \in \text{int}\{\mathbf{x} : f(\mathbf{x}) = \tilde{s}\}$, then there exists $\mathcal{B}(\mathbf{x}^*, r)$ with $f(\mathbf{x}) \equiv \tilde{s}$ for any $\mathbf{x} \in \mathcal{B}(\mathbf{x}^*, r)$, which indicates $\mathbf{0} \in \partial f(\mathbf{x}^*)$. By Fermat condition and the convexity of f , \mathbf{x}^* is an optimizer solution of f . However, with $f(\mathbf{x}^*) = \tilde{s} > f_{opt}$, the optimality of \mathbf{x}^* contradicts to the convexity. Hence, Φ_f cannot be discontinuous at $\tilde{s} \in (f_{opt}, \infty)$. Combined with (i) we can further derive that $\Phi_f(s)$ is upper semi-continuous for $s \in [f_{opt}, \infty)$, which completes the proof. \square

In the proof, if f is defined in \mathbb{R}^{l_f} , then $f : \mathbb{E} \rightarrow \mathbb{R}$ can also written as f' :

$$f'(\mathbf{x}) = \begin{cases} f(\mathbf{x}) + I_{\mathbb{E}}(\mathbf{x}), & \mathbf{x} \in \mathbb{E}, \\ I_{\mathbb{E}}(\mathbf{x}), & \mathbf{x} \notin \mathbb{E}, \end{cases}$$

where $I_{\mathbb{E}}$ is the indicator function defined by

$$I_{\mathbb{E}}(\mathbf{x}) = \begin{cases} 0, & \mathbf{x} \in \mathbb{E}, \\ \infty, & \mathbf{x} \notin \mathbb{E}. \end{cases}$$

C Proof of Theorem 6

Suppose there are two non-empty strict level sets $L_1 = \text{Lev}(f, s_1)$ and $L_2 = \text{Lev}(f, s_2)$, where $\Phi_f(s_1) = D_1$, $\Phi_f(s_2) = D_2$ and $D_2 > D_1 \geq \Phi_f(f_{opt}^+)$. Denote $\mathbf{x}^*(D_1) \in \text{cl}(L_1)$, $\mathbf{x}^*(D_2) \in \text{cl}(L_2)$ with $\mathbf{y}^*(L_1), \mathbf{y}^*(L_2)$

being their corresponding projection on X^* . Then, we have

$$\begin{aligned} 0 &\leq \|\mathbf{x}^*(L_2) - \mathbf{y}^*(L_2)\| - \|\mathbf{x}^*(L_1) - \mathbf{y}^*(L_1)\| \\ &\leq \|\mathbf{x}^*(L_2) - \mathbf{x}^*(L_1)\| + \|\mathbf{y}^*(L_2) - \mathbf{y}^*(L_1)\| \\ &\leq 2\|\mathbf{x}^*(L_2) - \mathbf{x}^*(L_1)\|. \end{aligned} \quad (\text{C.1})$$

By the boundness of X^* , $\Phi_f(f_{opt}^+) < \infty$ holds. We first prove (C.1) converges to 0 as $D_2 - D_1 \rightarrow 0$. Suppose there exist $\epsilon > 0$ which makes $\|\mathbf{x}^*(L_2) - \mathbf{y}^*(L_2)\| - \|\mathbf{x}^*(L_1) - \mathbf{y}^*(L_1)\| \geq \epsilon$ for any $D_2 > D_1 > D_{X^*}$, then utilize (C.1) we can obtain

$$\min \{\|\mathbf{x}^*(L_2) - \mathbf{x}^*(L_1)\|\} > \frac{\epsilon}{2}.$$

By the continuity of f , we can further obtain

$$\min \{\|\mathbf{x}^*(L_1) - \mathbf{x}^*(L_1)\|\} = 0 > \frac{\epsilon}{2}$$

as $D_2 \rightarrow D_1$, which contradicts to $\epsilon > 0$. Therefore, we can prove that

$$\max_{\mathbf{x} \in \text{cl}(\text{Lev}(f, s))} \|\mathbf{x} - \text{Proj}_{X^*}(\mathbf{x})\| \quad (\text{C.2})$$

is an upper semi-continuous mapping of D for

$$D \in [\Phi_f(f_{opt}^+), \Phi_f(+\infty)).$$

Moreover, by utilizing (C.2) we can obtain

$$\varphi(f_{opt}) = 0 = \varphi(f_{opt}^+), \quad (\text{C.3})$$

which complete the proof. \square